Rapid determination of erythrocyte sedimentation rate (ESR) by an electrically driven blood droplet biosensor

Cite as: Biomicrofluidics **14**, 064108 (2020); https://doi.org/10.1063/5.0026332
Submitted: 23 August 2020 . Accepted: 13 November 2020 . Published Online: 01 December 2020

Sumit Kumar, Rishi Ram, Arnab Sarkar, Sunando DasGupta, and Suman Chakraborty

Biomicrofluidics ARTICLE scitation.org/journal/bmf

Rapid determination of erythrocyte sedimentation rate (ESR) by an electrically driven blood droplet biosensor

Cite as: Biomicrofluidics 14, 064108 (2020); doi: 10.1063/5.0026332
Submitted: 23 August 2020 · Accepted: 13 November 2020 ·
Published Online: 1 December 2020

Sumit Kumar,[1] Rishi Ram,[2] Arnab Sarkar,[2,3] Sunando DasGupta,[1,4] and Suman Chakraborty[1,5,a)]

AFFILIATIONS

[1]Advanced Technology Development Centre, Indian Institute of Technology Kharagpur, Kharagpur, West Bengal 721302, India
[2]Department of Mechanical Engineering, Indian Institute of Technology (BHU), Varanasi, Uttar Pradesh 221005, India
[3]School of Medical Science and Technology, Indian Institute of Technology Kharagpur, Kharagpur, West Bengal 721302, India
[4]Department of Chemical Engineering, Indian Institute of Technology Kharagpur, Kharagpur, West Bengal 721302, India
[5]Department of Mechanical Engineering, Indian Institute of Technology Kharagpur, Kharagpur, West Bengal 721302, India

[a)]**Author to whom correspondence should be addressed:** suman@mech.iitkgp.ac.in. **Telephone:** +913222282990.
Fax: +913222282278

ABSTRACT

In healthcare practice, the sedimentation rate of red blood cells (erythrocytes) is a widely used clinical parameter for screening of several ailments such as stroke, infectious diseases, and malignancy. In a traditional pathological setting, the total time taken for evaluating this parameter varies typically from 1 to 2 h. Furthermore, the volume of human blood to be drawn for each test, following a gold standard laboratory technique (alternatively known as the Westergren method), varies from 4 to 5 ml. Circumventing the above constraints, here we propose a rapid (∼1 min) and highly energy efficient method for the simultaneous determination of hematocrit and erythrocyte sedimentation rate (ESR) on a microfluidic chip, deploying electrically driven spreading of a tiny drop of blood sample (∼8 μl). Our unique approach estimates these parameters by correlating the same with the time taken by the droplet to spread over a given radius, reproducing the results from more elaborate laboratory settings to a satisfactory extent. Our novel methodology is equally applicable for determining higher ranges of ESR such as high concentration of bilirubin and samples corresponding to patients with anemia and patients with some severe inflammation. Furthermore, the minimal fabrication steps involved in the process, along with the rapidity and inexpensiveness of the test, render the suitability of the strategy in extreme point-of-care settings.

INTRODUCTION

Erythrocyte sedimentation rate (ESR)[1–3] is a simple and widely used clinical test commonly used as an initial screening of various communicable and non-communicable diseases including prostate cancer,[1,4] stroke,[5] heart attack,[6] temporal arteritis,[7,8] and polymyalgia rheumatic.[9–12] In a physical sense, ESR indicates the rate of settling of erythrocyte in a vertical tube filled with whole blood. One hour later, the height of plasma (free from erythrocyte) at the uppermost portion of tube is measured and is traditionally described as the ESR value[1] in millimeters per hour. In the gold standard method for ESR measurement, known as Westergren method, a tube having 300 mm length and 2.50 mm inner diameter is used and 5–6 ml of a whole blood sample is required for clinical test.[1,13] ESR values above 30 mm/h are expected to correlate with a diseased condition and demand further clinical investigation.[1] Interestingly, the variation in ESR itself depends on physiological conditions such as hematocrit (HCT) and plasma protein level. ESR, at a low shear rate, also indicates the red blood cell (RBC) aggregation and viscosity of blood samples. Despite such far-reaching implications, one serious bottleneck still remains to be the fact that the conventional ESR measuring method suffers from several limitations, such as large volume consumption (∼5 ml), long measurement time (∼1 h), tiresome cleaning procedures, high cost due to bulky size of instruments, and difficulty in quality control.[14]

In the last few years, a number of new methods were proposed for determining the ESR using erythrocyte aggregation (EA). Erythrocyte aggregation is a physiological process where RBCs organize to form a face-to-face linear structure at a low shear rate, known as rouleaux.[1,15,16] Erythrocyte aggregation is influenced by many factors such as fibrinogen concentration in plasma, shear force on the cells, and cellular properties that include membrane deformability and surface charge density.[1,16–25] EA holds great potential in monitoring the progression of specific diseases like thrombosis, sepsis, and circulatory diseases.[15,26,27] Accordingly, this method has been used by several researchers.[1,16,33–36] In most of these studies, a photometric technique has been used to measure the aggregation of RBC.[18,28–32] Computational and image analysis of erythrocytes under different dynamic conditions have also been employed for the determination of EA.[1,16,28–31] EA can further be determined by measuring the volume, morphological properties, and refractive index of blood samples.[32–35] This method mainly relies on custom-made optical systems such as microscopes and holograms.[32–35] However, reported ESR measuring systems using EA are not very suitable for rapid monitoring and quantification of the fast aggregation process intrinsically encountered in medical practice.[36]

Microfluidic systems have been proven to hold a great potential in medical diagnostics and health monitoring when there is a need of low sample volume and rapid analysis.[1,16,37] A few years back, Isiksacan *et al.*[1] proposed a novel microfluidic system for predicting the ESR by measuring the rate of erythrocyte aggregation (EA). They demonstrated the rapid measurement of ESR using EA by utilizing the direct relationship between RBC aggregates and their settling speed. This microfluidic system is able to measure the ESR from EA using a volume of 40 μl whole blood in 2 min. In another microfluidic method,[14] it is reported that the ESR can also be determined by measuring the time duration of blood flow and the area of the depleted region of RBC through a microfluidic channel.

Though microfluidic platforms are portable and can, thus, be potentially used as point-of-care (POC) devices for ESR determination, microfluidic techniques reported for the said purpose involve complicated microfabrication. Relatively inexpensive microfluidic platforms, such as lab-on-a-compact disk, are, on the other hand, not energy efficient, as attributable to their large driving power necessary for flow actuation.[38,39] In addition, the volume of blood sample used in these devices is quite large. Therefore, it is very crucial to develop a novel droplet based microfluidic system for this purpose, which should be simple and easy to fabricate, very fast in execution, energy efficient, and necessitate only a minimal volume of the samples being investigated.

Here, we propose a simple and efficient technique on a chip for rapid determination of the hematocrit (volume fraction of the red blood cells) and ESR simultaneously, by exploiting the features of dynamic spreading of an 8 μl droplet of whole blood over a time span of 1 min under an applied electrical potential, as a mobile biosensor. Energy efficiency of the method stems from the fact that the electric potential is applied only for a very short span of time (2–3 s). The underlying principle of electrically driven dynamic spreading is simple[40–53] and operationally reproducible on a chip. In effect, we apply an electric potential across a blood droplet to record the change in its contact radius.[41,48,50,54–58] For a fixed change in the droplet radius, we measure different durations of time in achieving the same radius for different hematocrit levels of human blood samples. Using this varying temporal span and hematocrit level of blood, we subsequently determine the hematocrit level and ESR of a given blood sample. Such simultaneous determination of ESR and hematocrit level (or equivalently packed cell volume) holds outstanding importance in monitoring the progression of vector borne diseases such as dengue that may potentially become life-threatening for a large fraction of the global population. Our methodology has also been validated for determining higher ranges of ESR due to high concentration of bilirubin, anemia, and other severe inflammation.

EXPERIMENTAL DETAILS

Figure 1 depicts the experimental setup deployed for the purpose. For our experimental study, thin dielectric films of polydimethylsiloxane (PDMS) are coated on indium tin oxide (ITO)-coated rectangular glass slides. First, the glass slide with indium tin oxide coating is thoroughly cleaned by sonication, which is a well-known mechanism to remove particles from the surfaces. Sonication is carried out in two steps: first, ITO glass is sonicated with acetone for 15 min and then with de-ionized (DI) water for 15 min. Thereafter, it is dried using nitrogen (N_2) stream. The dielectric film is fabricated by mixing a cross-linker and a base in the weight ratio of 1:10 for 3–4 min. Thereafter, it is placed in a desiccator for half an hour to remove moisture, air-bubbles, and other gases. Next, the two-step spin coating method is used to fabricate the dielectric film using spin-coater. The electrode coated glass slide is placed on the vacuum chuck of the spin-coater, after covering a small portion of it using a parafilm tape. Then, the degassed, uncured PDMS is discharged cautiously over the uncoated portion of the glass slide and rotated at an angular acceleration 4000 rad/s^2 for 30 s at 500 rpm and 70 s at 3000 rpm. As a result, a thin film of PDMS is coated on the ITO glass slide. Once the coating of the thin film is carried out, the parafilm tape is removed to expose a small portion of the uncoated ITO electrode and subsequently cured overnight at 95 °C in the oven. The thickness of the dielectric film obtained is 30 μm when measured by a surface profilometer. The cleaning and fabrication process is shown in Fig. S1 in the supplementary material.

For carrying out experiments on blood samples, authorized consent from the Ethics Committee of the parent institute of the corresponding author was taken. For the clinical measurement of ESR, blood is used without any preprocessing. Therefore, the same fresh venous blood is taken from B C Roy Technology Hospital, Indian Institute of Technology Kharagpur, India, into cylindrical EDTA tubes to avoid coagulation. The hematocrit and ESR of the same blood sample have already been determined by the automated analyzer and Westergren method, respectively, in the aforesaid hospital, and the same sample is used for the simultaneous determination of hematocrit and ESR through electrically driven dynamic spreading in our setup (Fig. 1).

We perform our experiments on a microfluidic chip using sessile droplets of the whole human blood. The PDMS coated glass slide is mounted on the experimental setup (Fig. 1). Then, a sessile droplet of the blood (8 μl in volume) is carefully kept onto the hydrophobic surface with the help of a micropipet. The ITO glass

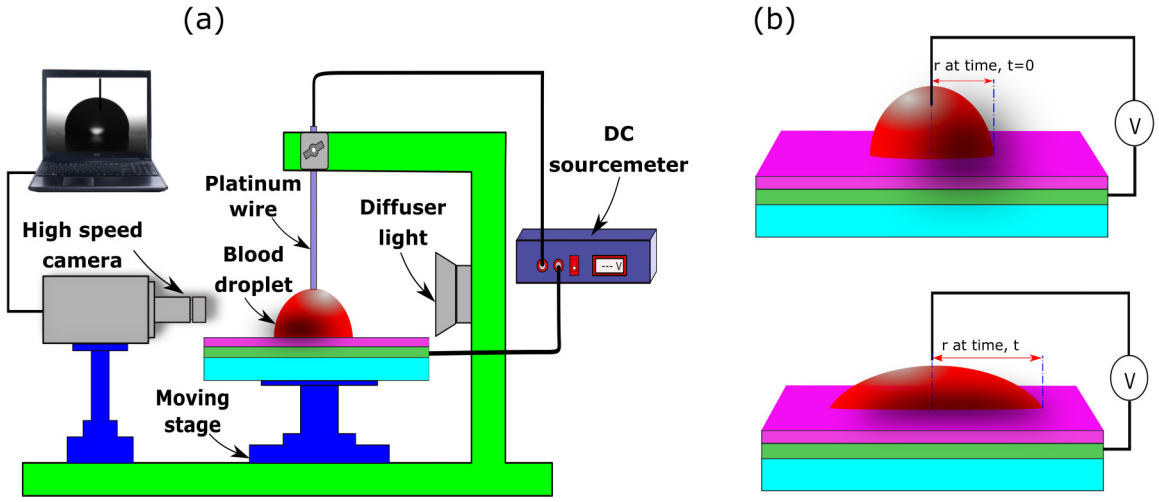

FIG. 1. (a) Schematic electrospreading based microfluidic system for the rapid determination of ESR and hematocrit level of whole blood. (b) Blood droplet at time t = 0 without electric field and at time t with electric field.

slide is electrically kept on ground state, and the electrical circuit is completed through platinum wire electrode (diameter 200 μm) dipped into the blood droplet. The schematic depiction of the experimental setup is shown in Fig. 1. An electrical sourcemeter is used to apply an electrical potential between the platinum wire and the ITO electrode. On the application of the DC electrical potential, the blood droplet spreads on the dielectric film till the final equilibrium is reached, and the successive images of the blood droplet spreading are taken using a camera at 2000 frames per second. Each experiment is repeated thrice for the same blood sample at the same voltage. Experiments are carried out at voltages ranging from 200 V to 600 V for different blood samples with varying hematocrit levels. Variation of initial contact angle, initial contact radius, and contact angle hysteresis with the hematocrit level are given in Figs. S2–S4 in the supplementary material. From the graphs, it is very clear that the effect of hematocrit level of the blood on the initial contact angle, initial contact radius, and contact angle hysteresis is almost negligible. In addition, the variation of the static contact angle with applied voltage is given in Fig. S5 in the supplementary material. Contact angle of the blood droplet decreases with voltage for different hematocrit levels of blood samples. In this figure, electrical voltage has been increased from 0 V to 200 V. The contact angle of the droplet is non-dimensionalized with its initial contact angle (β_0). Initial contact angles for different blood samples are as follows: β_0 (HCT: 45%) = 107.96°; β_0 (HCT: 41%) = 105.36°; β_0 (HCT: 37%) = 105.7°, and β_0 (HCT: 34.9%) = 105.1°. The electrical voltage is normalized by the final applied voltage (V = 200 V). The surface tension coefficients of different blood samples are given in Table I. Figure 2 shows the variation of viscosity (mPa s) with the shear rate (s^{-1}) for different hematocrit levels of blood samples. From the plot, it is evident that all blood sample exhibit a shear-thinning behavior under the applied shear rate. The variation of the flow consistency index (k) and the flow behavior index (n) with the hematocrit level and ESR of blood samples are given in Figs. 3 and 4, respectively.

RESULTS AND DISCUSSION

In the present electrospreading based portable microfluidic system, a DC electrical potential is applied across the sessile droplet of the whole blood, and subsequently, the image sequence of the droplet deformation is recorded using a high-speed camera. It is worthy to mention that we can also apply AC potential instead of DC. However, it has been reported that in case of AC electrowetting, the electric field may get remarkably reduced in the dielectric layer near the contact line, leading to a decrease of the electrostatic contribution to the wetting tension.[40] Since in the present biosensor the electrostatic contribution to the wetting tension is of utmost importance, we have applied DC potential instead of AC.

TABLE I. The variation of the surface tension with the hematocrit level.

Hematocrit level, HCT (%)	Surface tension (γ, mN/m)
27	50.13
29	51.29
32	53.36
36	54.10
38.1	52.42
42.1	50.30
43.9	54.18
45.2	49.22
47	53.24
48.7	51.42

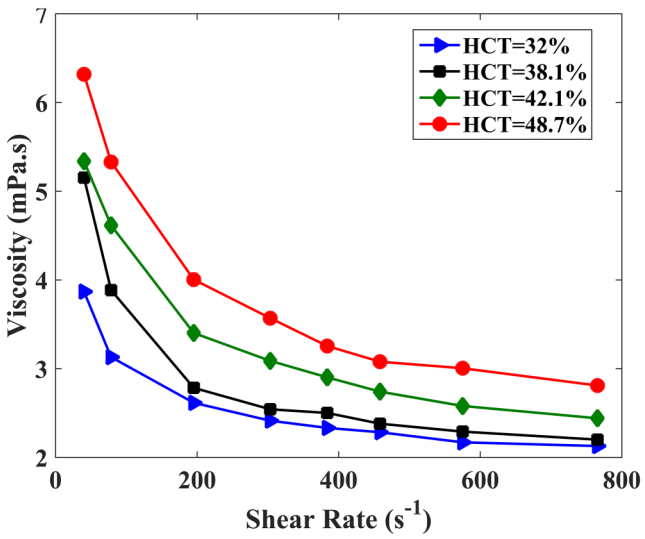

FIG. 2. Variation of the viscosity (mPa s) with the shear rate (s^{-1}) for different hematocrit level of blood samples.

The images of blood droplets are post-processed using an image processing software, and the evolution of the contact radius with time is measured for different hematocrit (HCT) levels (HCT). The spreading rate of a blood drop decreases with the increase in the hematocrit level of the blood (Fig. 5). The reason behind this observation may be due to augmentation in the viscosity of blood with the increasing hematocrit level[66] (Fig. 3).

Since an electrically driven spreading method[50,59–82] is used to predict the ESR and hematocrit level of blood samples, it is essential to discuss in brief the physics involved with the same. When an electric field is imposed across the droplet, the solid–liquid interfacial energy is tailored, and the contact radius of conducting droplet increases and the contact angle decreases with time and finally reaches an equilibrium state.[41,48,50,54–58] In other words, from the electromechanical perspective, when an electrical potential is imposed across the conducting droplet, an electrical stress develops near the three phase contact line (TPCL), which pushes the contact line away from the droplet center and subsequently droplet spreads.[83] During this process, the electrical forces have to overcome the counteracting viscous forces acting at the three phase contact line (TPCL). Hence, the rate of spreading of a Newtonian droplet can further be altered by changing the viscosity of the fluid as the contact line friction enhances with an increase in the viscosity of the droplets.[84–88] Hong *et al.*[86] have investigated the effect of viscosity and droplet size on the dynamic behavior of electrowetting. Their study reveals that the friction coefficient is a strong function the viscosity of fluids. However, the applied electrical potential and the droplet size rarely influence the contact line friction coefficient. Later, they studied the effect of oil viscosity and droplet size on the dynamic spreading characteristics of sessile droplets in an oil pool under applied DC electric field.[87] The settling time has been found to be a function of the droplet radius and the oil viscosity.[87] Therefore, during the last three decades, this technique has evolved as a feasible, promising, and a remarkably efficient approach in digital microfluidics (DMF) to manipulate droplet radius and apparent contact angle by altering the interfacial energy or electrical stress at TPCL, with applications ranging from variable focal liquid lens to lab-on-chip devices and a new type of electronic display to cooling systems,[54–58,89–94] although its true potential is yet to be harnessed in medical diagnostic applications.

Since blood is an inhomogeneous, polarized, anisotropic, and composite fluid, it generally exhibits a strikingly distinct behavior from a Newtonian fluid. In simpler form, blood follows a power law constitutive relation, which can be written as $\tau_{xy} = k\left(\frac{du}{dy}\right)^n$,

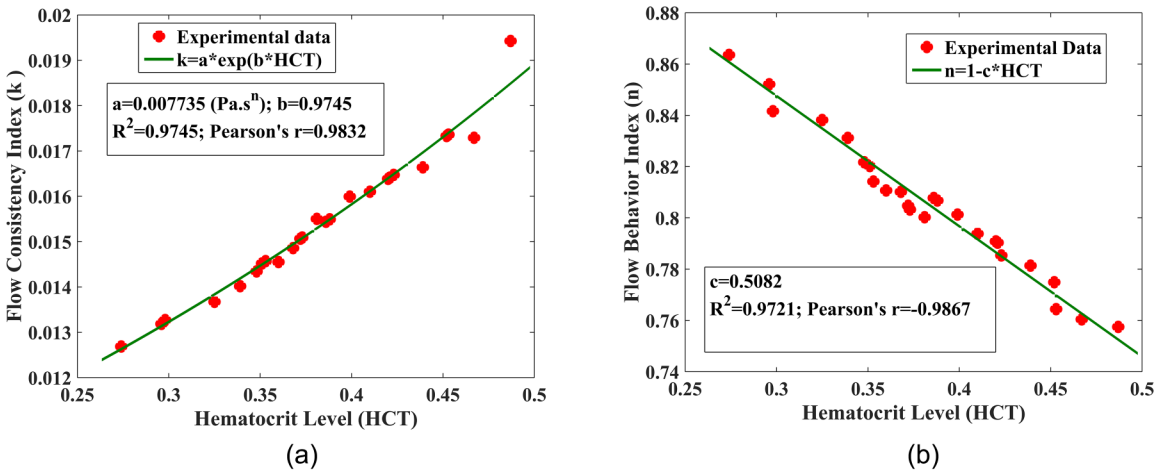

FIG. 3. Variation of (a) flow consistency index (k) and (b) flow behavior index (n) with hematocrit (HCT) level of different blood samples.

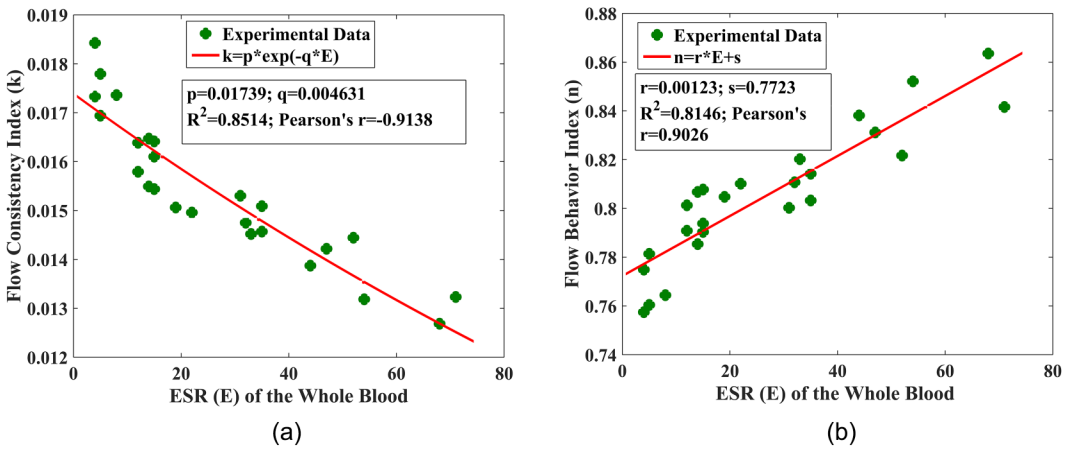

FIG. 4. Variation of (a) flow consistency index (k) and (b) flow behavior index (n) with ESR (E) of different blood samples.

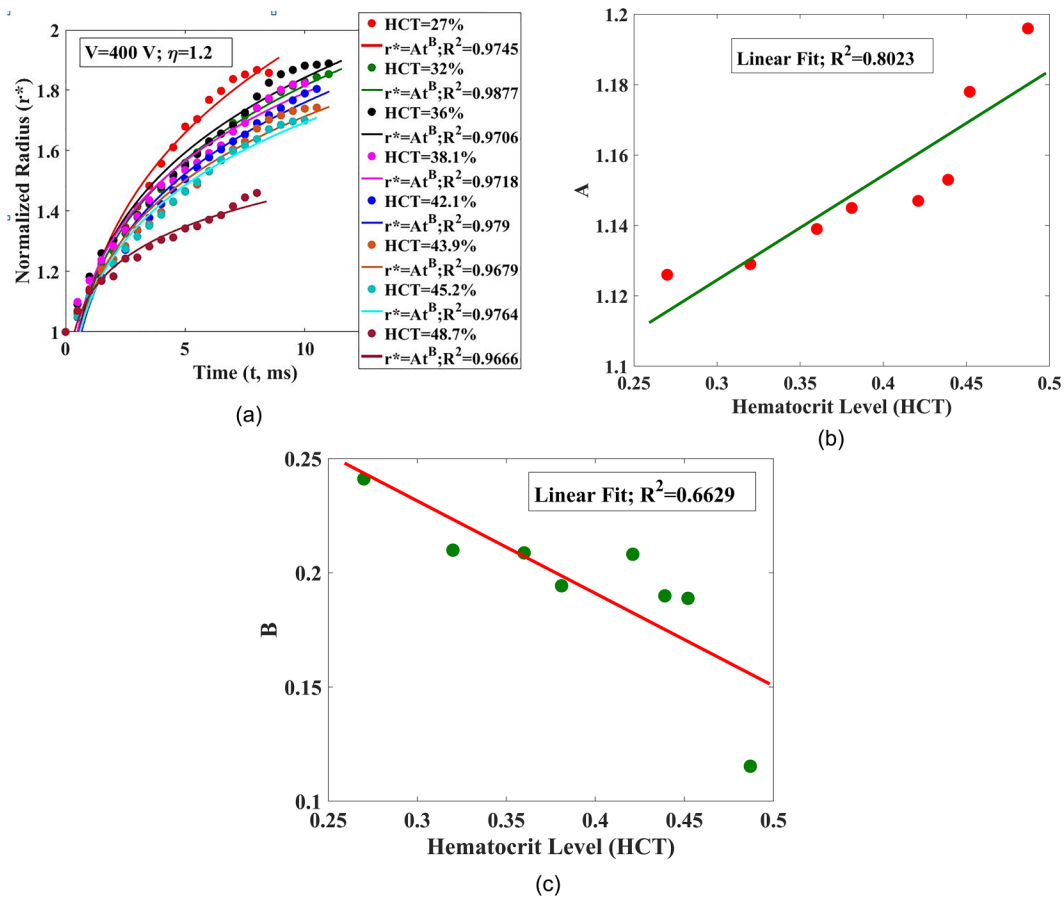

FIG. 5. (a) Variation of normalized contact radius with time. (b) and (c) Variation of the prefactor (A) and the power law exponent (B) with the hematocrit level of blood samples for a fixed electrowetting number.

where k and n represent the flow consistency index and flow behavior index, respectively.[95,96] It is already established that the values of k and n strongly depend on the hematocrit (HCT) level (which is basically a volume fraction of red blood cells in blood samples) by following the rheological relation given as $k = a \times \exp(b \times HCT)$ and $n = 1 - c \times HCT$[96] (Fig. 3). Our experimental results show a good quantitative agreement with this reported empirical relation.[96,97] The values of a, b, and c are given in Fig. 3. In addition, we also propose an empirical relation using the rheometry results that directly relate the ESR with the rheological parameters (k and n) for different blood samples (Fig. 4).

From the above discussion, it can be concluded that the hematocrit level of a blood sample plays a very dominating role in determining the blood viscosity, as depicted in Fig. 3. Therefore, variations in the hematocrit level of blood may significantly alter the velocity profile near the three phase contact line of a blood droplet, which, in turn, may have a strong influence on the viscous dissipation during spreading.[95] Hence, viscous action, which primarily depends on the blood rheology,[95] plays a major role in modulating the spreading rate of blood, in addition to the strength of the electrical field (Figs. 5 and 6). This spreading of blood droplet is basically due to a combination of two effects: the primary effect is the electrospreading of blood droplet, the physics of which has already been discussed, and the secondary effect is blood rheology, manifested by blood viscosity for which hematocrit plays a crucial role. Since the spreading of the blood droplet is driven solely by the electric field, it is governed by the deformability of erythrocyte (RBC). RBCs are the major cellular component of blood, and they are highly deformable. However, the tendency of RBCs to form rouleaux and move together as aggregates may increase under the application of the electric field, which restricts further spreading of the blood droplet.[98–100] This augmentation in rouleaux formation may be due to the enhanced deformation of RBCs caused by applied electrical potential.[101,102] This is when the secondary effect

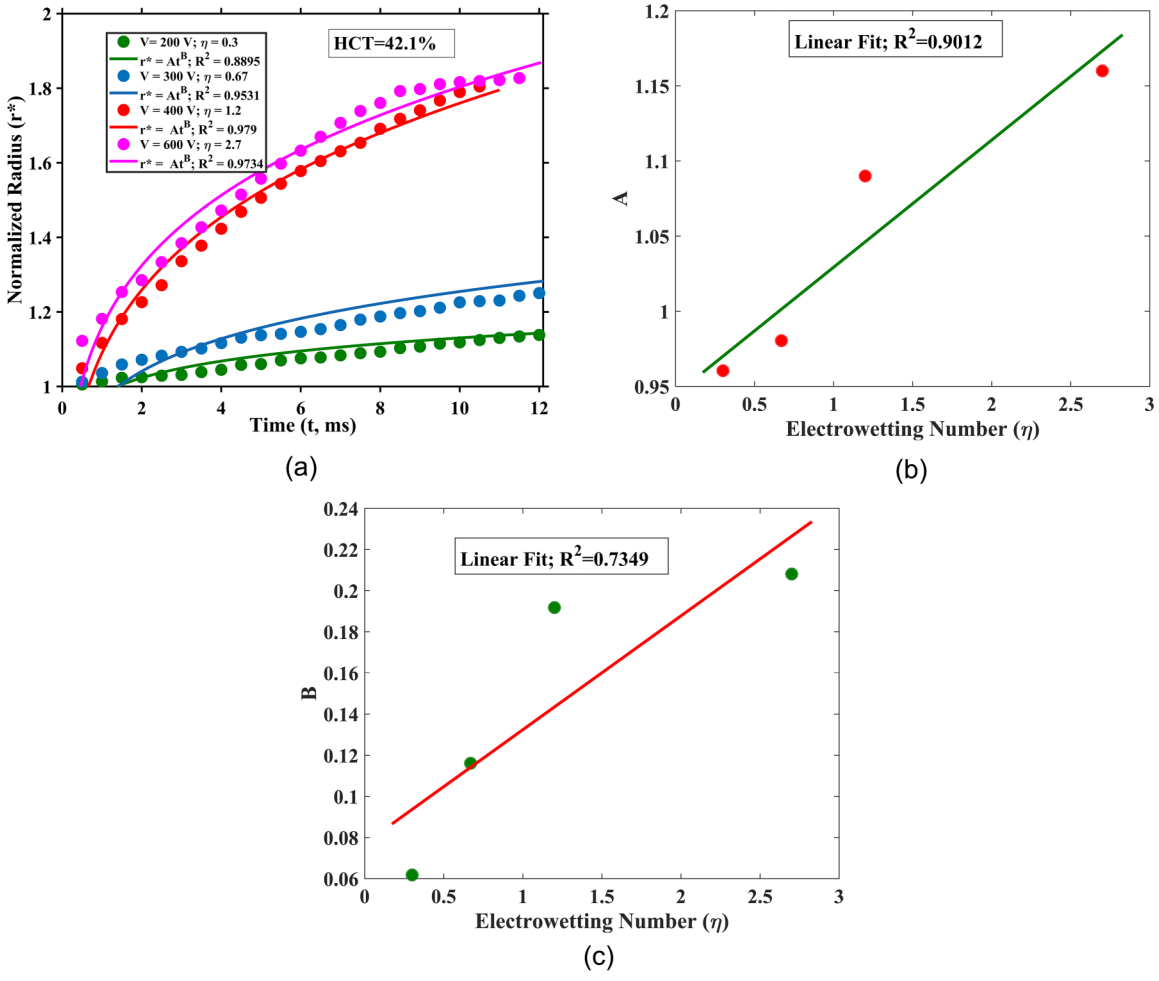

FIG. 6. (a) Variation of normalized contact radius with time. (b) and (c) variation of the prefactor (A) and the power law exponent (B) with the electrowetting number for a fixed blood sample.

of blood rheology comes into play. Red blood cells exhibiting shear-thinning effect and for their rouleaux formation, the spreading of the blood droplet will not begin due to enhanced viscous action until sufficient electric potential is available, rendering the temporal change of radius of blood being directly correlated with its hematocrit level.

As observed experimentally, the temporal change of radius of blood with varying hematocrit levels under electrospreading follows a power law relationship, $r = At^B$, where A and B depend upon the hematocrit (HCT) level of whole blood (Fig. 5). This is true when viscous action dominates over the electric field. However, for fixed blood samples, it has also been observed that the values of A and B are functions of the electrowetting number only (Fig. 6), especially when electric field predominates viscous action. Electrowetting number is defined as the ratio of electrical force to the surface tension force and can be written as $\eta = \frac{\varepsilon_0 \varepsilon_r}{2\gamma h} V^2$, where ε_0 is the permittivity of free space, ε_r is the dielectric contact of PDMS material, γ is the surface tension of liquid, h is the thickness of the PDMS film, and V is the applied voltage.[40,52] To summarize, it may be inferred that the spreading rate of blood is modulated by electrical forces acting at the three phase contact line due to the applied electrical voltage, along with the rheology of blood, which further depends upon the hematocrit level and ESR of blood samples.

It becomes imperative to understand the interplay of forces while determining ESR traditionally, and its relationship with the present method. In the traditional Westergren method, forces acting on blood are the gravity force, viscous force, and buoyant force. The sedimentation of erythrocyte is governed by the particle sedimentation theory[1,16] where gravity force is balanced by viscous force and buoyant force. ESR basically indicates how quickly red blood cells settle in the tube. According to the particle sedimentation theory, the Stokes law renders the settling or sedimentation velocity and is given as

$$V = \frac{2g}{9} \frac{(\rho_{RBC} - \rho_{plasma})}{\mu} r^2, \tag{1}$$

where ρ_{RBC} and ρ_{plasma} are the densities of red blood cell (RBC) and plasma, respectively, μ is the blood viscosity, and r is the radius of RBC. Hence, the difference in the density, erythrocyte radius, and blood viscosity are the determinants of sedimentation velocity.

It has been found that blood viscosity mainly depends on the hematocrit level.[96] However, it has also been observed that blood viscosity further depends on fibrinogen and other plasma proteins, especially at low shear rates.[103,104] It has been reported that for some patients, blood viscosity measured at a high shear rate was significantly correlated with the hematocrit level, whereas blood viscosity determined at a low shear rate was not correlated with the hematocrit level.[1] It has been found that internal viscosity of red blood cells and whole blood viscosity decreases with the increase in the plasma fibrinogen concentration over a very large range of shear rates.[105,106] Hence, apart from the hematocrit level, fibrinogen and other plasma protein concentrations play a crucial role in determining blood viscosity. Such complex rheological considerations may turn out to be of significant consequence in several other applications of interfacial transport phenomena over small scales.[107–115]

In the present method for determining ESR, a blood droplet spreads due to the application of an electric field, which is the body force replacing gravity force in traditional devices. Under equilibrium condition, this electric force is balanced by viscous force. It may be noted that buoyant force would be absent in this platform. However, in this system, ESR is dependent on blood viscosity, which, in turn, depends on the hematocrit level as well as

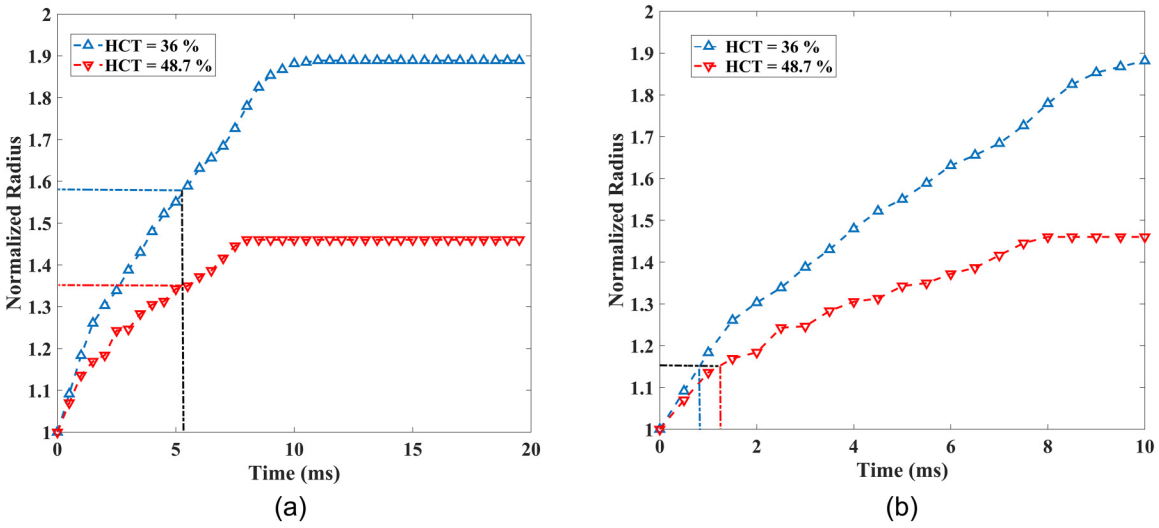

FIG. 7. (a) Normalized radii of the blood droplets of different hematocrit at a fixed time, t = 5.5 ms. (b) Time taken by the blood droplets of different hematocrit to attain a fixed normalized radius r* = 1.15 (shown only for six samples).

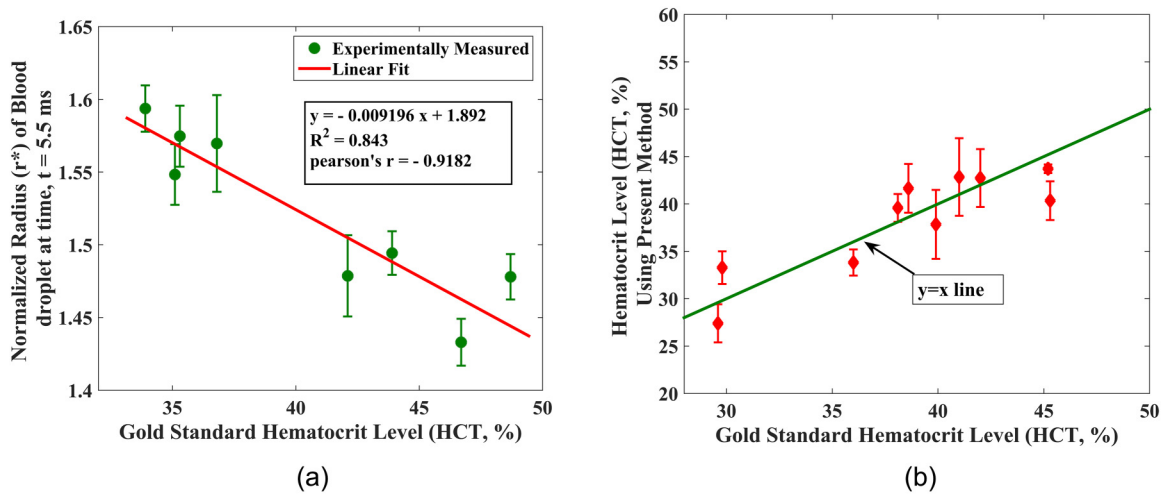

FIG. 8. (a) The variation of normalized droplet radius at time t = 5.5 ms with varying hematocrit (HCT) levels of the blood sample at electric potential = 400 V. (b) Comparison of hematocrit levels of different blood samples measured using our microfluidic method with the gold standard method.

fibrinogen and other protein concentrations. Since fibrinogen and other plasma protein concentrations influence blood viscosity, these are also able to influence the ESR. When there is inflammation in the body, fibrinogen and other plasma protein concentrations increase, rendering an increase in ESR. Hence, ESR is a non-specific measurement of degree of inflammation. However, we can also interpret ESR as the indication of how quickly red blood cells settle in the traditional Westergren tube or how quickly droplets spread in reaching a particular radius in our proposed electrically driven biosensor. When there is inflammation, the spreading of red blood cells becomes relatively quicker due to the increase of fibrinogen and other protein concentrations. This quick spreading can be additionally contributed by RBC membrane viscoelasticity and red blood cell morphology. Hence, in Eq. (2), apart from hematocrit, ESR is also considered function of the duration of blood droplet spreading (T) in reaching a fixed radius, and this duration decreases under inflammatory condition rendering a corresponding increase in the ESR. In order to further assess the effectiveness of the present method, we have considered some blood samples where the hematocrit levels are the same and the ESR only

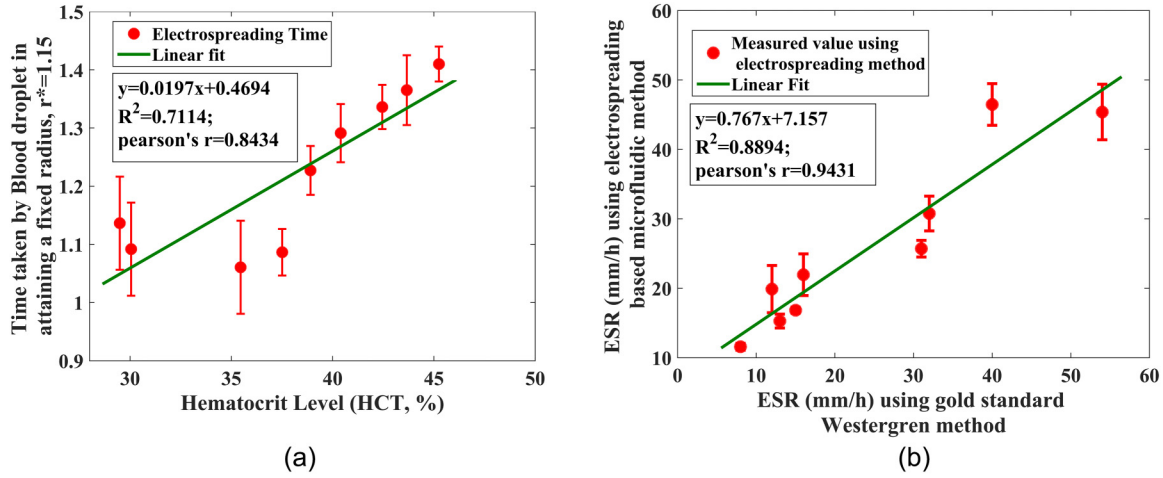

FIG. 9. (a) The variation of time (ms) taken by a droplet in attaining a fixed normalized radius r* = 1.15 with varying hematocrit (HCT) fraction at 400 V. (b) Comparison of the measured ESR results using an electrospreading based microfluidic method (*y* axis) with the gold standard Westergren method. ESRs of 11 venipuncture whole blood samples are determined using the gold standard Westergren method (*x* axis). The R^2 and Pearson's r values of linear fit are 0.9431 and 0.904, respectively.

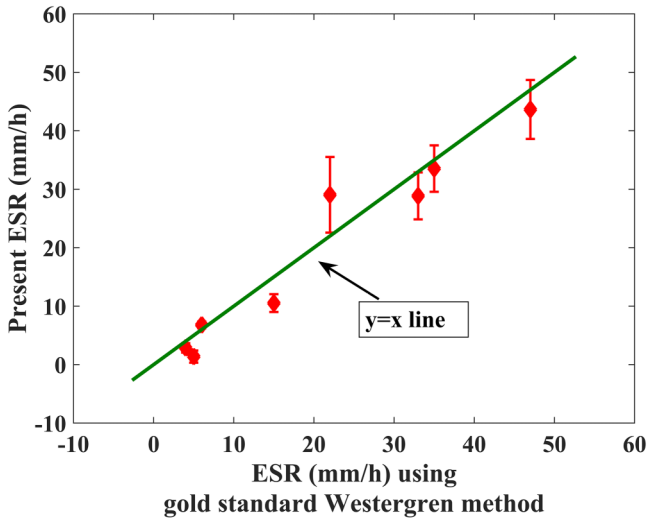

FIG. 10. Precision test for the electrospreading based microfluidic system. The ESRs of seven whole blood samples are determined using the gold standard Westergren method (*x* axis) and then each sample is tested with our microfluidic method (*y* axis). The standard deviation is also shown in the figure.

varies. ESR values measured using the present method have been in excellent quantitative agreement with ESR values measured using the gold standard device (see Fig. S6 in the supplementary material) for all such cases.

For our method, the following correlation of ESR determination in terms of hematocrit (HCT) level and the duration of blood droplet spreading (T) in reaching a fixed radius can be written[101] as

$$ESR = k_1 T^{-1}(1 - HCT)^2 10^{-1.82 \times HCT}. \quad (2)$$

where k_1 is the calibration constant. Such a simple correlation of morphological and rheological parameters not only turns out to be of utilitarian importance in the specific application addressed in this work but also turns out to be of extreme fundamental importance toward establishing a generic principle of analyzing transport mechanisms in a wide variety of applications ranging from microfluidics to materials engineering and physiology.

Now, we measure the normalized radius of blood droplets at a particular time, t = 5.5 ms, for different hematocrit levels [Figs. 7(a) and 8(a)], and subsequently, a linear relation is developed between the gold standard hematocrit level and radius of drop ($R^2 = 0.843$, Pearson's r = −0.9182). Using Eq. (2), we further predict the hematocrit level of a new set of seven blood samples by knowing the radius of spreading at the particular time, t = 5.5 ms [Fig. 8(b)]. We observe a good agreement between the present and the gold standard results.

From Fig. 8, we have observed the variation of hematocrit with normalized radius under a specific electric field. Since for a given electric field normalized radius and time are interdependent, we have not explicitly considered time while determining hematocrit or equivalently packed cell volume. Next, we measure the time (*T*) taken by droplets of a set of blood samples to reach a particular normalized radius (∼1.15) [Figs. 7(b) and 9(a)] and using these time durations and previously measured hematocrit levels of blood samples, we determine the ESR of the respective blood sample using Eq. (2), where k_1 is 10 000. A linear relationship has been established among ESR values determined with the help of Eq. (2)

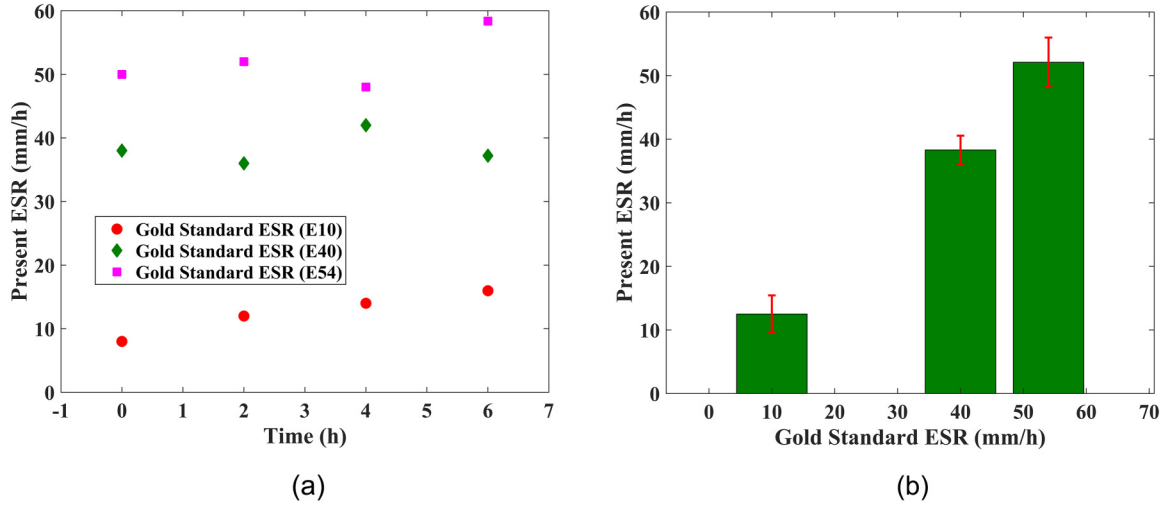

FIG. 11. (a) Performance test of the electrospreading based microfluidic method. (a)The ESR of three blood samples (ESR = 10, 40, and 54 mm/h) are first measured with the gold standard method, and then our microfluidic method is used to test the ESRs of whole blood samples with 2 h delay between successive tests. (b) The average value of ESR and standard deviation using present method is measured and compared with the gold standard Westergren method.

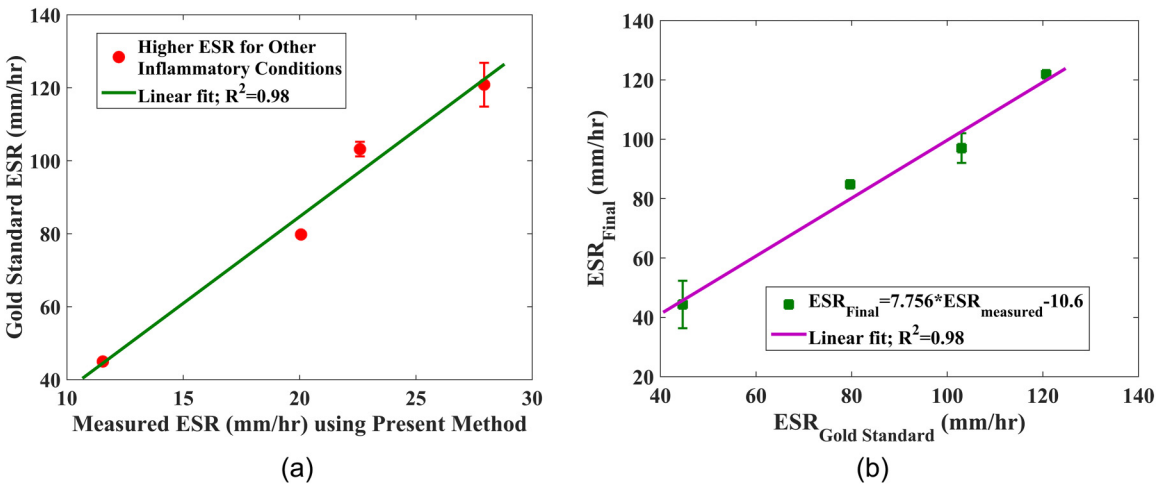

FIG. 12. (a) Comparison of the average value of ESR using the present method with the gold standard Westergren method for the cases like high concentration of triglycerides, cholesterol, and bilirubin; samples corresponding to patients with anemia; or other severe inflammation conditions. (b) Calibration curve for determining ESR in higher ranges, and ESR values after calibration (ESR_{Final}) have been found to have an excellent agreement with ESR values measured by the gold standard technique.

and ESR values measured using the gold standard Westergren method [Fig. 9(b)]. The values of R^2 and Pearson's r for linear fit in Fig. 9(b) have been found as 0.8894 and 0.9431, respectively.

After establishing the linear relation that is used to calculate the ESR values using the hematocrit (HCT) level determined from Fig. 8(b) and from the time taken in achieving a fixed droplet radius [using Fig. 9(a)], the performance capability of our electrospreading based microfluidic system is further evaluated. First of all, we test the precision of our microfluidic system. The ESRs of eight blood samples are first measured using the gold standard method (Westergren method) and are found as 4, 5, 6, 15, 22, 33, 35, and 47 mm/h (Fig. 10, *x* axis). Now using hematocrit levels of blood measured from Fig. 8(a) along with the time elapsed in achieving a fixed radius of blood, we determine the ESRs of eight blood samples using our microfluidic method [Fig. 9(b)]. The mean values obtained are 2.86, 1.37, 6.79, 10.52, 29.04, 33.53, 28.86, and 43.64 mm/h (Fig. 10, *y* axis), whereas the standard deviations of these samples are 4.96, 2.11, 5.05, 3.46, 2.86, 3.38, and 2.64, respectively, and are shown in Fig. 10 as error bars. This precision test reveals an excellent agreement between the present and gold standard results.

In clinical research, it is also very crucial to investigate the performance of a device when a delay happens between the consecutive tests as the time gap between the blood samples taken from a patient and testing in the pathology lab fluctuates from a few minutes to 3–4 h. It is observed that this time delay reveals a variation in ESR not only among different pathology labs but also within the same lab. It is, therefore, very important to test the repeatability of the method for blood samples stored in EDTA tubes for different time periods. We have taken the blood samples of three patients with ESR values of 10, 40, and 54 mm/h for performing the repeatability test. These blood samples are further used to measure the ESRs using our microfluidic method over the span of 6 h, with a 2 h interval between two readings [Fig. 11(a)].

Also, the proposed microfluidic method is used to determine the mean and standard deviation of three measured ESR values of a blood sample with an ESR value of 10, 40, and 54 mm/h as per the gold standard device. The mean and standard deviation for all three blood samples using our present method are found as 12.49 (E10), 2.94; 38.3 (E40), 2.25; and 52.09 (E54), 3.89 [Fig. 11(b)]. This repeatability test further confirms that there are no significant changes in the ESR values of blood samples even after 6 h.

We also validate the applicability of our methodology for determining significantly higher ranges of ESR due to severe inflammatory conditions, high concentration of bilirubin, and anemia. It has already been reported that the performance of another portable microfluidic device for measuring ESR drastically deteriorates while handling higher ranges of ESR (>30 mm/h). In that case, the coefficient of determination (R^2) sharply reduces from 0.79, which has been found while correlating with lower ranges of ESR (≤30 mm/h), to 0.69.[1] However, in sharp contrast with this reported finding, our methodology is found to be equally applicable for higher ranges of ESR. Our calibration curve for determining ESR in higher ranges is depicted in Fig. 12, and ESR values after calibration (ESR_{Final}) have been found to have an excellent agreement with the ESR values measured by the gold standard device, rendering R^2 as 0.98. Hence, our methodology has been proved to be validated for both lower and higher ranges of ESR.

CONCLUSIONS

We have developed a droplet based portable microfluidic sensor premised on electrically driven dynamic spreading of a droplet for the simultaneous determination of the hematocrit and ESR levels from a tiny volume of a blood sample at a rapid rate. Our results exhibit excellent agreement with the gold standard Westergren method and exhibits excellent repeatability under varying conditions.

At the same time, our proposed device is able to confiscate the deficiencies of the gold standard method such as large sample volume consumption, long time in completing the test, operator related constraints like tube shaking and tube positioning, and considerable energy consumption. In addition, our method is not fabrication intensive, free from vibration, and can be implemented through the design of a portable device. With such benefits, our methodology has been proved to be highly sensitive for determining higher ranges of ESR, which can further be exploited for developing a point-of-care (POC) device for identifying severe inflammatory conditions and monitoring infectious and other life-threatening diseases through the measurement of ESR in resource constrained settings.

SUPPLEMENTARY MATERIAL

See the supplementary material for the cleaning procedure and fabrication steps in Fig. S1. The variations of initial contact angle, contact radius, and contact angle hysteresis with hematocrit levels of blood are provided in Figs. S2–S4, respectively. The variation of the static contact angle with applied voltage is given in Fig. S5. Furthermore, the comparison of the gold standard ESR and the present ESR for blood samples of the same hematocrit level is shown in Fig. S6.

ACKNOWLEDGMENTS

S.C. acknowledges the Department of Science and Technology, Government of India, for Sir J. C. Bose National Fellowship. S.K. and R.R. gratefully acknowledge Mr. Rajib Das of the B C Roy Technology Hospital for supplying the biological samples.

DATA AVAILABILITY

The data that support the findings of this study are available from the corresponding author upon reasonable request.

REFERENCES

[1]Z. Isiksacan, O. Erel, and C. Elbuken, Lab Chip **16**, 4682 (2016).
[2]A. Grzybowski and J. Sak, Clin. Dermatol. **29**, 697 (2011).
[3]A. Westergren, Acta Med. Scand. **54**, 247 (1921).
[4]J.-E. Johansson, T. Sigurdsson, L. Holmberg, and R. Bergstrom, Cancer **70**, 1556 (1992).
[5]A. Singh, V. Atam, B. Yathish, L. Das, and S. Koonwar, J. Neurosci. Rural Pract. **5**, 40 (2014).
[6]M. B. Andresdottir, N. Sigfusson, H. Sigvaldason, and V. Gudnason, Am. J. Epidemiol. **158**, 844 (2003).
[7]M. R. Cheema and S. Ismaeel, Clin. Interv. Aging **2016**, 185.
[8]R. L. Wong and J. H. Korn, Am. J. Med. **80**, 959 (1986).
[9]H. C. Sox and M. H. Liang, Ann. Intern. Med. **104**, 515 (1986).
[10]F. Wolfe, J. Rheumatol. **22**, 788 (1995).
[11]S. M. Helfgott and R. I. Kieval, Arthritis Rheumatol. **39**, 304 (1996).
[12]M. Plebani and E. Piva, Am. J. Clin. Pathol. **117**, 621 (2002).
[13]S. E. Bedell and B. T. Bush, Am. J. Med. **78**, 1001 (1985).
[14]Y. J. Kang, Y. R. Ha, and S. J. Lee, Biomicrofluidics **8**, 034110 (2014).
[15]O. Baskurt, B. Neu, and H. J. Meiselman, *Red Blood Cell Aggregation* (CRC Press, 2011).
[16]Z. Isiksacan, M. Asghari, and C. Elbuken, Microfluid. Nanofluid. **21**, 1 (2017).
[17]H. Jung Lim, Y. J. Lee, J. H. Nam, S. Chung, and S. Shin, J. Biomech. **43**, 546 (2010).
[18]O. K. Baskurt, M. Uyuklu, S. Ozdem, and H. J. Meiselman, Clin. Hemorheol. Microcirc. **47**, 295 (2011).
[19]S. Shin, J. H. Nam, J. X. Hou, and J. S. Suh, Clin. Hemorheol. Microcirc. **42**, 117 (2009).
[20]G. Barshtein, I. Tamir, and S. Yedgar, Eur. Biophys. J. **27**, 177 (1998).
[21]M. Boynard and J. C. Lelievre, Biorheology **27**, 39 (1990).
[22]N. Maeda and T. Shiga, BBA Gen. Subj. **843**, 128 (1985).
[23]G. B. Nash and H. J. Meiselman, Biorheology **22**, 73 (1985).
[24]N. Maeda, M. Seike, T. Nakajima, Y. Izumida, M. Sekiya, and T. Shiga, BBA Biomembr. **1022**, 72 (1990).
[25]B. Neu, R. Wenby, and H. J. Meiselman, Biophys. J. **95**, 3059 (2008).
[26]O. K. Baskurt, A. Temiz, and H. J. Meiselman, J. Lab. Clin. Med. **130**, 183 (1997).
[27]O. K. Baskurt and H. J. Meiselman, Clin. Hemorheol. Microcirc. **53**, 23 (2013).
[28]S. Chen, G. Barshtein, B. Gavish, Y. Mahler, and S. Yedgar, Clin. Hemorheol. Microcirc. **14**, 497 (1994).
[29]S. Jayavanth and M. Singh, ITBM-RBM **25**, 67 (2004).
[30]G. Barshtein, D. Wajnblum, and S. Yedgar, Biophys. J. **78**, 2470 (2000).
[31]S. Chen, B. Gavish, S. Zhang, Y. Mahler, and S. Yedgar, Biorheology **32**, 487 (1995).
[32]T. Kim, R. Zhou, M. Mir, S. D. Babacan, P. S. Carney, L. L. Goddard, and G. Popescu, Nat. Photonics **8**, 256 (2014).
[33]D. Dannhauser, D. Rossi, F. Causa, P. Memmolo, A. Finizio, T. Wriedt, J. Hellmers, Y. Eremin, P. Ferraro, and P. A. Netti, Lab Chip **15**, 3278 (2015).
[34]S. Mavandadi, S. Feng, F. Yu, S. Dimitrov, K. Nielsen-Saines, W. R. Prescott, and A. Ozcan, PLoS One **7**, e46192 (2012).
[35]B. Rappaz, P. Marquet, E. Cuche, Y. Emery, C. Depeursinge, and P. J. Magistretti, Opt. Express **13**, 9361 (2005).
[36]L. Miccio, P. Memmolo, F. Merola, P. A. Netti, and P. Ferraro, Nat. Commun. **6**, 6502 (2015).
[37]D. P. Manage, Y. C. Morrissey, A. J. Stickel, J. Lauzon, A. Atrazhev, J. P. Acker, and L. M. Pilarski, Microfluid. Nanofluid. **10**, 697 (2011).
[38]S. Kar, M. Dash, T. K. Maiti, and S. Chakraborty, Analyst **140**, 1432 (2015).
[39]R. Agarwal, A. Sarkar, and S. Chakraborty, Analyst **144**, 3782 (2019).
[40]F. Mugele and J.-C. Baret, J. Phys. Condens. Matter **17**, R705 (2005).
[41]D. Baratian, R. Dey, H. Hoek, D. Van Den Ende, and F. Mugele, Phys. Rev. Lett. **120**, 214502 (2018).
[42]D. Chakraborty, G. S. Sudha, S. Chakraborty, and S. DasGupta, J. Colloid Interface Sci. **363**, 640 (2011).
[43]G. McHale, C. V. Brown, M. I. Newton, G. G. Wells, and N. Sampara, Phys. Rev. Lett. **107**, 186101 (2011).
[44]G. McHale, C. V. Brown, and N. Sampara, Nat. Commun. **4**, 1605 (2013).
[45]Z. Brabcova, G. McHale, G. G. Wells, C. V. Brown, and M. I. Newton, Appl. Phys. Lett. **110**, 121603 (2017).
[46]J. C. Baret and F. Mugele, Phys. Rev. Lett. **96**, 1 (2006).
[47]F. Mugele, Soft Matter **5**, 3377 (2009).
[48]R. De Ruiter, C. Semprebon, M. Van Gorcum, M. H. G. Duits, M. Brinkmann, and F. Mugele, Phys. Rev. Lett. **114**, 234501 (2015).
[49]R. Dey, S. Dasgupta, and S. Chakraborty, Microfluid. Nanofluid. **21**, 1 (2017).
[50]J. Gao, N. Mendel, R. Dey, D. Baratian, and F. Mugele, Appl. Phys. Lett. **112**, 203703 (2018).
[51]R. Dey, U. U. Ghosh, S. Chakraborty, and S. DasGupta, Langmuir **31**, 11269 (2015).
[52]R. Dey, A. Daga, S. Dasgupta, and S. Chakraborty, Appl. Phys. Lett. **107**, 16 (2015).
[53]S. Kumar, P. Kumar, S. DasGupta, and S. Chakraborty, Appl. Phys. Lett. **114**, 073702 (2019).
[54]L. Chen, C. Li, N. F. A. Van Der Vegt, G. K. Auernhammer, and E. Bonaccurso, Phys. Rev. Lett. **110**, 026103 (2013).
[55]J. Liu, M. Wang, S. Chen, and M. O. Robbins, Phys. Rev. Lett. **108**, 216101 (2012).
[56]Y. Yamamoto, T. Ito, T. Wakimoto, and K. Katoh, J. Fluid Mech. **839**, 468 (2018).
[57]G. Manukyan, J. M. Oh, D. Van Den Ende, R. G. H. Lammertink, and F. Mugele, Phys. Rev. Lett. **106**, 014501 (2011).

[58]D. Sun and K. F. Böhringer, Appl. Phys. Lett. **116**, 093702 (2020).
[59]S. Högnadóttir, K. Kristinsson, H. G. Thormar, and K. Leosson, Appl. Phys. Lett. **116**, 073702 (2020).
[60]E. D. Wikramanayake, J. Perry, and V. Bahadur, Appl. Phys. Lett. **116**, 193701 (2020).
[61]R. Yan, T. S. McClure, I. H. Jasim, A. K. R. Koppula, S. Wang, M. Almasri, and C.-L. Chen, Appl. Phys. Lett. **113**, 204101 (2018).
[62]C. Palma and R. Deegan, Appl. Phys. Lett. **106**, 014106 (2015).
[63]D. J. Preston, A. Anders, B. Barabadi, E. Tio, Y. Zhu, D. A. Dai, and E. N. Wang, Appl. Phys. Lett. **109**, 244102 (2016).
[64]C. Enrico Clement and S.-Y. Park, Appl. Phys. Lett. **108**, 191601 (2016).
[65]J. Ha, J. Park, Y. Kim, B. Shin, J. Bae, and H.-Y. Kim, Phys. Fluids **28**, 102102 (2016).
[66]M. Strauch, P. A. A. M. Somers, F. Bociort, and H. P. Urbach, AIP Adv. **8**, 115224 (2018).
[67]S. Lv, C. Liu, and W. Luo, AIP Adv. **8**, 115035 (2018).
[68]F. Ribet, E. De Luca, F. Ottonello-Briano, M. Swillo, N. Roxhed, and G. Stemme, Appl. Phys. Lett. **115**, 073502 (2019).
[69]M. Torabinia, A. Farzbod, and H. Moon, J. Appl. Phys. **123**, 154902 (2018).
[70]H. Xu, R. Yan, S. Wang, and C.-L. Chen, Phys. Fluids **29**, 102105 (2017).
[71]X. Tan, Z. Tao, K. Suzuki, and H. Li, AIP Adv. **7**, 125212 (2017).
[72]X. Ren, S. Wei, X. Qu, and F. Liu, AIP Adv. **9**, 055021 (2019).
[73]J.-M. Löwe, J. Plog, Y. Jiang, Y. Pan, and A. L. Yarin, J. Appl. Phys. **126**, 035302 (2019).
[74]M. Strauch, Y. Shao, F. Bociort, and H. P. Urbach, Appl. Phys. Lett. **111**, 171106 (2017).
[75]J. Zheng, Y. Cheng, Y. Huang, S. Wang, L. Liu, and G. Chen, Phys. Fluids **32**, 097108 (2020).
[76]X. He, J. Zhang, X. Zhang, and Y. Deng, Soft Matter **15**, 5211 (2019).
[77]C. Jiang, H. Ma, D. G. Hasko, and A. Nathan, Appl. Phys. Lett. **109**, 211601 (2016).
[78]T. He, M. Jin, J. C. T. Eijkel, G. Zhou, and L. Shui, Biomicrofluidics **10**, 011908 (2016).
[79]F. Yang, R. A. Shaw, C. W. Gurganus, S. K. Chong, and Y. K. Yap, Appl. Phys. Lett. **107**, 264101 (2015).
[80]H. A. A. Ali, H. A. Mohamed, and M. Abdelgawad, Biomicrofluidics **9**, 014115 (2015).
[81]Y. Guan, B. Li, and L. Xing, Phys. Fluids **30**, 112001 (2018).
[82]Z. Li, J. Li, and H. Chen, Appl. Phys. Lett. **113**, 243702 (2018).
[83]S. Kumar, S. DasGupta, and S. Chakraborty, Phys. Fluids **21**, 112001 (2020).
[84]Q. Vo and T. Tran, Phys. Rev. E **97**, 063101 (2018).
[85]Q. Vo, H. Su, and T. Tran, Sci. Rep. **8**, 836 (2018).
[86]J. Hong, Y. K. Kim, K. H. Kang, J. M. Oh, and I. S. Kang, Langmuir **29**, 9118 (2013).
[87]J. Hong, Y. K. Kim, K. H. Kang, J. Kim, and S. J. Lee, Sens. Actuators B Chem. **196**, 292 (2014).
[88]J. Hong, Y. K. Kim, K. H. Kang, J. Kim, and S. J. Lee, Sens. Actuators B Chem. **190**, 48 (2014).
[89]M. Li, C. Dong, M. K. Law, Y. Jia, P. I. Mak, and R. P. Martins, Sens. Actuators B Chem. **287**, 390 (2019).
[90]X. Li, H. Feng, Y. Wang, C. Zhou, W. Jiang, M. Zhong, and J. Zhou, Sens. Actuators B Chem. **262**, 411 (2018).
[91]K. N. Nampoothiri, M. S. Seshasayee, V. Srinivasan, M. S. Bobji, and P. Sen, Sens. Actuators B Chem. **273**, 862 (2018).
[92]C. Li, K. Zhang, X. Wang, J. Zhang, H. Liu, and J. Zhou, Sens. Actuators B Chem. **255**, 3616 (2018).
[93]F. Ribet, L. De Pietro, N. Roxhed, and G. Stemme, Sens. Actuators B Chem. **267**, 647 (2018).
[94]A. T. Jafry, H. Lee, A. P. Tenggara, H. Lim, Y. Moon, S. H. Kim, Y. Lee, S. M. Kim, S. Park, D. Byun, and J. Lee, Sens. Actuators B Chem. **282**, 831 (2019).
[95]A. Carré and P. Woehl, Langmuir **22**, 134 (2006).
[96]S. Chakraborty, Lab Chip **5**, 421 (2005).
[97]S. Das and S. Chakraborty, Anal. Chim. Acta **559**, 15 (2006).
[98]D. Patel, T. C. Ford, and D. Rickwood, *Cell Separation: A Practical Approach* (Oxford University Press, Oxford, 1998), see https://books.google.co.in/books/about/Cell_Separation.html?id=GSWudM-1XGcC&redir_esc=y.
[99]Y. Takamura, K. Idegami, M. Kogi, and H. Takabayashi, U.S. patent 9,334,477 B2 (10 May 2016), see https://patentimages.storage.googleapis.com/61/23/e5/9c0b6fee78070d/US9334477.pdf.
[100]Z. T. F. Yu, J. G. Joseph, S. X. Liu, M. K. Cheung, P. J. Haffey, K. Kurabayashi, and J. Fu, Sens. Actuators B Chem. **245**, 1050 (2017).
[101]H. Engelhardt, H. Gaub, and E. Sackmann, Nature **307**, 378 (1984).
[102]P. Scheurich, U. Zimmermann, M. Mischel, and I. Lamprecht, Z. Naturforsch. C **35**, 1081 (1980).
[103]T. Matsuda and M. Murakami, Thromb. Res. **8**, 25 (1976).
[104]R. Ishak and K. Hassan, Med. J. Malaysia **40**, 191 (1985).
[105]P. A. Dupont and J. A. Sirs, Thromb. Haemost. **38**, 0660 (1977).
[106]L. Dintenfass, *Blood Viscosity* (MTP Press, 1985).
[107]S. Chakraborty and A. K. Srivastava, Langmuir **23**(24), 12421 (2007).
[108]P. Goswami, J. Chakraborty, A. Bandopadhyay, and S. Chakraborty, Microvasc. Res. **103**, 41 (2016).
[109]R. Dua and S. Chakraborty, Comput. Biol. Med. **35**(5), 447 (2005).
[110]N. Chakraborty and S. Chakraborty, Int. J. Heat Mass Transfer **50**(9–10), 1805 (2007).
[111]U. Rana, S. Chakraborty, and S. K. Som, Energy **68**, 510 (2014).
[112]A. Bandopadhyay, S. Mandal, N. K. Kishore, and S. Chakraborty, J. Fluid Mech. **792**, 553 (2016).
[113]R. Dey, D. Chakraborty, and S. Chakraborty, J. Heat Transfer **133**(2), 024503 (2011).
[114]S. Chakraborty and S. Padhy, ACS Nano **2**(10), 2029 (2008).
[115]S. Chakraborty and F. Durst, Phys. Fluids **19**(8), 088104 (2007).